RSC Advances

PAPER

View Article Online
View Journal | View Issue

Cite this: *RSC Adv.*, 2018, **8**, 30825

Facile synthesis of high-performance SiO_2@Au core–shell nanoparticles with high SERS activity†

Keli Wang,‡[ab] Yanping Wang,‡[b] Chongwen Wang,*[bc] Xiaofei Jia,[b] Jia Li,[b] Rui Xiao*[ab] and Shengqi Wang*[ab]

Received 18th June 2018
Accepted 28th August 2018

DOI: 10.1039/c8ra05213a

rsc.li/rsc-advances

This study proposes a facile and general method for fabricating a wide range of high-performance SiO_2@Au core–shell nanoparticles (NPs). The thicknesses of Au shells can be easily controlled, and the process of Au shell formation was completed within 5 min through sonication. The fabricated SiO_2@Au NPs with highly uniform size and SERS activity could be ideal SERS tags for SERS-based immunoassay.

The design and controlled fabrication of Au nanocomposites have attracted extensive attention because of their outstanding chemical and optical properties and wide applications in various fields, such as catalysis,[1] drug delivery,[2] photothermal cancer therapy,[3] sensing,[4] and surface-enhanced Raman scattering (SERS).[5] However, small Au nanocomposites tend to aggregate, which seriously affects their stability and usability. The combination of silica nanoparticles (SiO_2 NPs) and Au shells provides a good alternative to Au nanocomposites.[6,7] These SiO_2 NPs are ideal core materials due to their high stability, easy preparation, uniform spherical shape, and large particle size range.[8,9]

Many synthesis methods have been explored for the fabrication of SiO_2@Au core–shell NPs; these methods include electroless plating,[10] self-assembly,[11] layer-by-layer synthesis,[12] and seed growth.[13] The seed growth method is the most commonly used to coat the Au shell on the surface of the SiO_2 core and involves two steps: deposition of nucleus seeds on the functionalized SiO_2 surface and Au shell growth. Although this method is beneficial for the synthesis of nanostructures with narrow size distribution, it exhibits two major shortcomings. First, the surface of SiO_2 NPs must be functionalized with various organosilanes containing amino ($-NH_2$) or mercapto (–SH) groups for adsorption or deposition of metal seeds on the SiO_2 NPs before subsequent growth of Au shells.[14,15] However, full surface amino/mercapto modification is often difficult to achieve; in this regard, dense metal seed layer formation on the surface of SiO_2 NPs cannot be achieved, eventually affecting the uniform and complete Au shell coating. Second, the formation of complete Au shell on the SiO_2 NPs is frequently achieved using a slow-growth approach through slow or multiple addition of $HAuCl_4$ to the seed-coated SiO_2 NPs suspension containing reducing agents.[16,17] The application of these slow-growth methods is restricted by its complex procedure and time-consuming preparation. Thus, a facile method must be developed for synthesis of Au coated SiO_2 NPs with controllable Au shell, good dispersibility, and fast preparation.

In this work, we report a sonochemically assisted seed growth method for facile synthesis of monodisperse SiO_2@Au core–shell NPs for the first time. Cationic polyethyleneimine (PEI) was used to form a cationic thin interlayer with numerous primary amine groups for easy adsorption of dense Au seeds on the silica surface and keeping the nanostructure stability during shell growth. Sonication was used instead of traditionally used mechanical stirring to shorten the reaction time. The entire reaction process for Au shell formation was completed within 5 min. Moreover, the thickness of the Au shell was easily controlled outside the silica cores of different sizes. To the best of our knowledge, the proposed method is the most convenient synthesis route for preparation of high-performance SiO_2@Au core–shell NPs to date. Our results further demonstrate that the fabricated SiO_2@Au NP could be an ideal SERS tag for SERS-based lateral flow immunoassay (LFA). The method was validated for detection of human immunoglobulin M (IgM) and showed a detection limit as low as 0.1 ng mL^{-1}. The details of the experiments including SiO_2@Au NPs preparation, SERS-based LFA strip preparation, SERS detection protocol, and sensitivity test were provided in the ESI† section.

The synthesis principle of monodisperse SiO_2@Au NPs is presented in Fig. 1a. SiO_2 NPs were first prepared by using a modified Stöber method as the core. The SiO_2 NPs were ultrasonically treated with PEI solution to form PEI-coated SiO_2 NPs (SiO_2@PEI). The positively charged PEI effectively attached to the negatively charged SiO_2 NPs and formed a stable polymer layer *via* electrostatic self-assembly. SiO_2–Au seed NPs were prepared by adsorbing small Au NPs (3–5 nm) on the PEI layer of

[a]*Anhui Medical University, Hefei, 230032, PR China. E-mail: sqwang@bmi.ac.cn; ruixiao203@sina.com*

[b]*Beijing Institute of Radiation Medicine, Beijing 100850, PR China. E-mail: wangchongwen1987@126.com*

[c]*College of Life Science, Anhui Agricultural University, Hefei 230036, China*

† Electronic supplementary information (ESI) available. See DOI: 10.1039/c8ra05213a

‡ Authors Keli Wang and Yanping Wang contributed equally to this work.

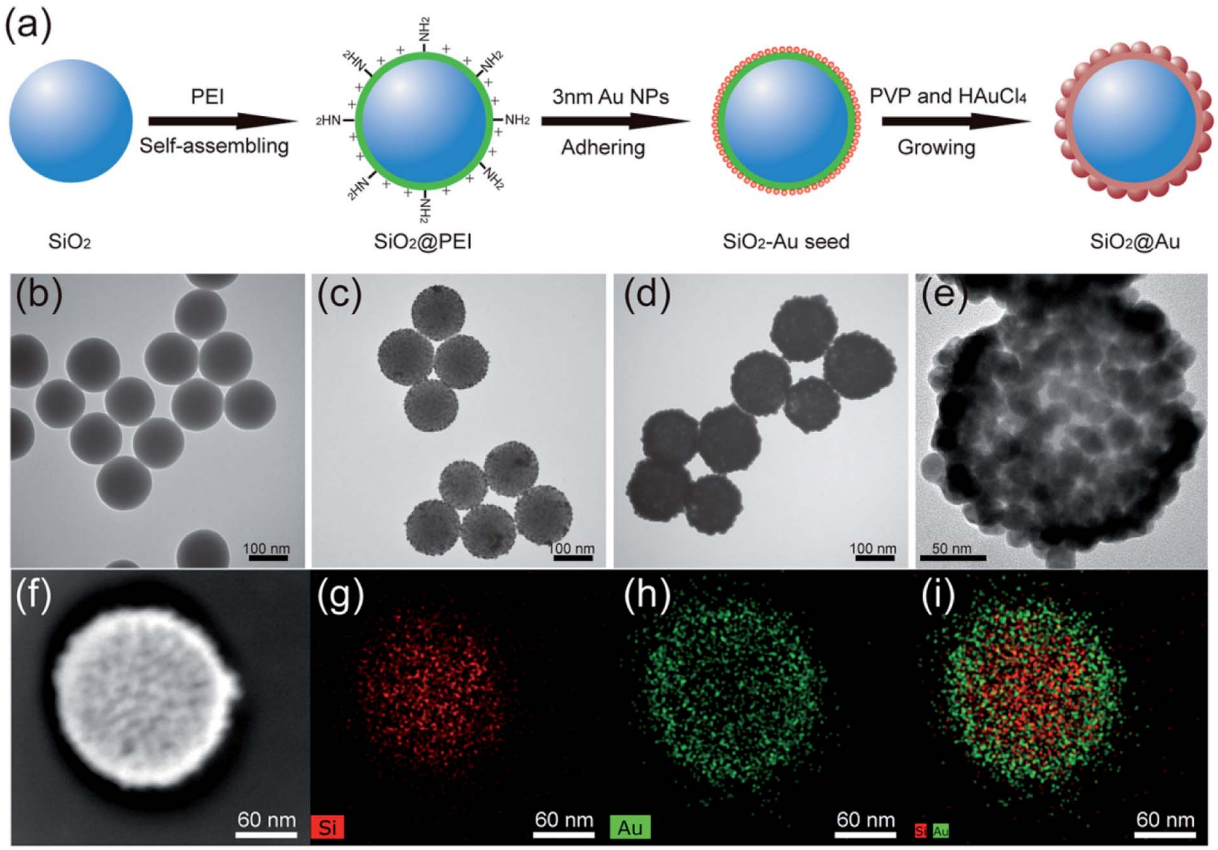

Fig. 1 Synthesis principle of SiO_2@Au NPs (a). TEM images of (b) SiO_2 NPs, (c) SiO_2–Au seed NPs, (d) SiO_2@Au NPs and their corresponding elemental mapping in (g), (h), and (i) respectively. (e) HRTEM picture and (f) bright-field TEM image of a single SiO_2@Au NP.

SiO_2 NPs densely and firmly through covalent binding between the $-NH_2$ groups of PEI and Au NPs. Finally, monodisperse SiO_2@Au NPs were quickly obtained through the reduction of $HAuCl_4$ by hydroxylamine hydrochloride ($NH_2OH \cdot HCl$) under the stabilization of PVP. The uniform Au shells outside the SiO_2 NPs were formed within 5 minutes through the isotropic growth of all Au seeds under sonication.

The morphology of the as-synthesized products in different stages were characterized through transmission electron microscopy (TEM). The as-prepared SiO_2 NPs were uniform in size and had a diameter of approximately 140 nm (Fig. 1b). After coating the SiO_2@PEI NPs with Au seeds, many small seeds homogeneously adhered to the surface of the silica core (Fig. 1c). The dense Au seeds acted as randomly oriented crystalline sites for subsequent seed-mediated growth of the Au shell. Fig. 1d and e show the low- and high-magnification TEM images of the final SiO_2@Au core–shell NPs, respectively. Continuous and rough edges were detected around the SiO_2@Au NPs. The HRTEM image (Fig. 1e) indicated that large adjacent Au NPs covered the entire surface of the SiO_2 NPs, forming a complete and rough Au shell. The average particle size increased from 140 nm to 190 nm after the Au shell formation, indicating that the thickness of the Au shell was approximately 25 nm. Additionally, the SEM images (Fig. S1†) showed that the SiO_2@Au NPs were successfully fabricated on a large scale and exhibited a rough surface and uniform size. The elemental composition of SiO_2@Au NPs was also confirmed through X-ray mapping (Fig. 1f–i). The results indicated that a layer of Au shell was uniformly coated on the surface of the SiO_2 NPs. The zeta potentials of SiO_2, SiO_2@PEI, SiO_2–Au seeds, and SiO_2@Au NPs in aqueous solution were found to be −46.7, +41.9, −7.4, and −21.1 mV, respectively (Fig. S2†). The significant change in the zeta potential revealed the successive completion of PEI coating, Au seed adsorption, and Au shell formation.

Fig. 2a shows the typical XRD patterns of the as-synthesized SiO_2–Au seed (blue line) and SiO_2@Au NPs (red line). The specific XRD pattern of Au is characterized by five peaks positioned at 2θ values of 38.3°, 44.3°, 64.5°, 77.4°, and 81.6°, which correspond to the reflections of the (111), (200), (220), (311), and (222) crystalline planes of Au (JCPDS no. 04-0784), respectively.[18,19] The intensity of the diffraction peaks of SiO_2@Au NPs increased when the Au shells were coated. No peaks of SiO_2 and PEI were detected in the XRD pattern because of their amorphous form.[20]

Fig. 2b illustrates the UV-vis spectra of the as-synthesized products dispersed in deionized water in different stages. SiO_2 and SiO_2@PEI NPs had no obvious absorption peaks in the UV-vis spectra (curves a and b). SiO_2–Au seed NPs displayed a clear absorption peak at about 568 nm (curve c), which confirms the

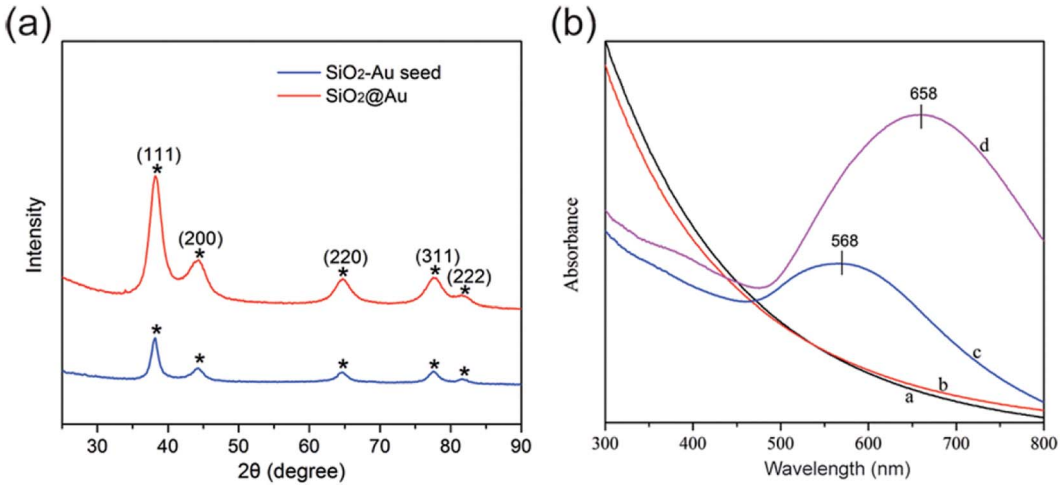

Fig. 2 Typical XRD patterns (a) and UV-visible spectra (b) of the as-synthesized products.

formation of the Au seed layer onto the surface of SiO_2 NPs. As the Au shell formed, the UV-vis spectral peak obviously red-shifted, and the intensity increased significantly (curve d). This result could be due to the strong interaction between and the coupling of the large adjacent Au NPs of the Au shells outside the SiO_2 NPs.[21]

The strategy for Au shell formation is essentially seed-mediated growth. Thus, the surface morphology of SiO_2@Au NPs can be easily controlled by adjusting the Au^{3+} concentration by using a constant amount of SiO_2–Au seed. Fig. 3a–d shows the representative TEM images of SiO_2@Au NPs synthesized with different concentrations of $HAuCl_4$ while the other parameters remained constant. As the concentration of the $HAuCl_4$ increased from 0.01 mM to 0.04 mM, the Au seeds absorbed outside the SiO_2 NPs gradually increased in size and finally intersected with each other and formed a continuous and Au shell of a different thickness.

Fig. 3e shows the UV-vis spectra of the synthesized SiO_2–Au seed and SiO_2@Au NPs with different Au shell thicknesses. The absorption peak of the obtained products red shifted gradually from 568 nm to 700 nm, and the peak width became broader with increasing concentration of $HAuCl_4$. Thus, the absorption peak of SiO_2@Au NPs can also reflect the formation and thickness of the Au shell.

Fig. 3f shows the SERS activity of SiO_2@Au NPs prepared with different $HAuCl_4$ concentrations. 5,5-Dithiobis-(2-nitrobenzoic acid) (DTNB) was used as Raman molecule because it contains a double sulfur bond, which can be chemically coupled to the Au shell to form Au–S chemical bond and could produce strong and concise SERS peaks located at 1062, 1148, 1331, and 1556 cm^{-1}.[22,23] Moreover, DTNB molecules can provide free carboxyl groups as sites to conjugate antibodies.[24] As shown in the Raman spectra in Fig. 3f, the SiO_2–Au seed showed fairly weak SERS ability (spectra a), whereas the SiO_2@Au NPs exhibited gradually enhanced SERS activity as the $HAuCl_4$ concentration increased (spectra b–d). However, the overgrowth of the Au shell decreased the SERS activity of SiO_2@Au NPs (spectra e). This phenomenon could be attributed to the fully continuous Au shell formation, which reduced the nanogaps and hot spots on the surface of SiO_2@Au NPs. Hence, we chose SiO_2@Au NPs prepared with 0.02 mM $HAuCl_4$ as the optimal material for SERS application because of their nearly complete Au shell and optimal enhancement effect.

PEI can be self-assembled on the surface of SiO_2 NPs of any size under sonication conditions. Thus, our proposed PEI-assisted seed growth method is a general route for preparing monodisperse SiO_2@Au core–shell particles with different sizes, ranging from nanoscale to microscale levels. Fig. 4a–c shows the TEM images of single SiO_2–Au seed NPs with different sizes (70–300 nm), and Fig. 4d–f clearly shows their corresponding fabricated SiO_2@Au NPs, respectively. The TEM images of multiple SiO_2@Au NPs with different sizes are displayed in Fig. S3.† All of the obtained SiO_2@Au NPs possess homogeneous nanostructure, uniform Au nanoshell, and good dispersity. We further examine the dependence of SERS activity on the SiO_2@Au NPs size up to 350 nm. Fig. S4† shows a set of SERS spectra of DTNB (10^{-5} M) adsorbed on the SiO_2@Au NPs of different sizes. The SERS intensity presented in the figure is the average intensity from 10 spots for each sample. Obviously, all the SiO_2@Au NPs exhibited excellent SERS abilities, and the signal intensities were gradually enhanced as the particle size increased. In fact, the Au shells of SiO_2@Au NPs were made of large sized Au NPs. This experimental result indicates that the larger the size of the Au NPs of shell, the higher the SERS activity achieved.

For the determination of the SERS sensitivity of the 80 nm SiO_2@Au NPs, a series of DTNB ethanol solution (with concentration ranging from 10^{-4} M to 10^{-11} M) was prepared. Each tube of DTNB solution was mixed with 10 μL of SiO_2@Au NPs (1 mg mL^{-1}) and sonicated for 1 h. After separation and washing, the final precipitate was dropped on a Si chip and analyzed with Raman signals. The spectra and calibration curve of DTNB absorbed on the SiO_2@Au NPs are shown in Fig. 5a and b, respectively. The SERS signal significantly decreased as the concentration of DTNB decreased, and the main Raman peak at 1331 cm^{-1} remained evident at DTNB concentrations as low as 10^{-10} M. Thus, the limit of detection (LOD) of DTNB is 10^{-10} M. These results indicate that the SiO_2@Au NPs have good

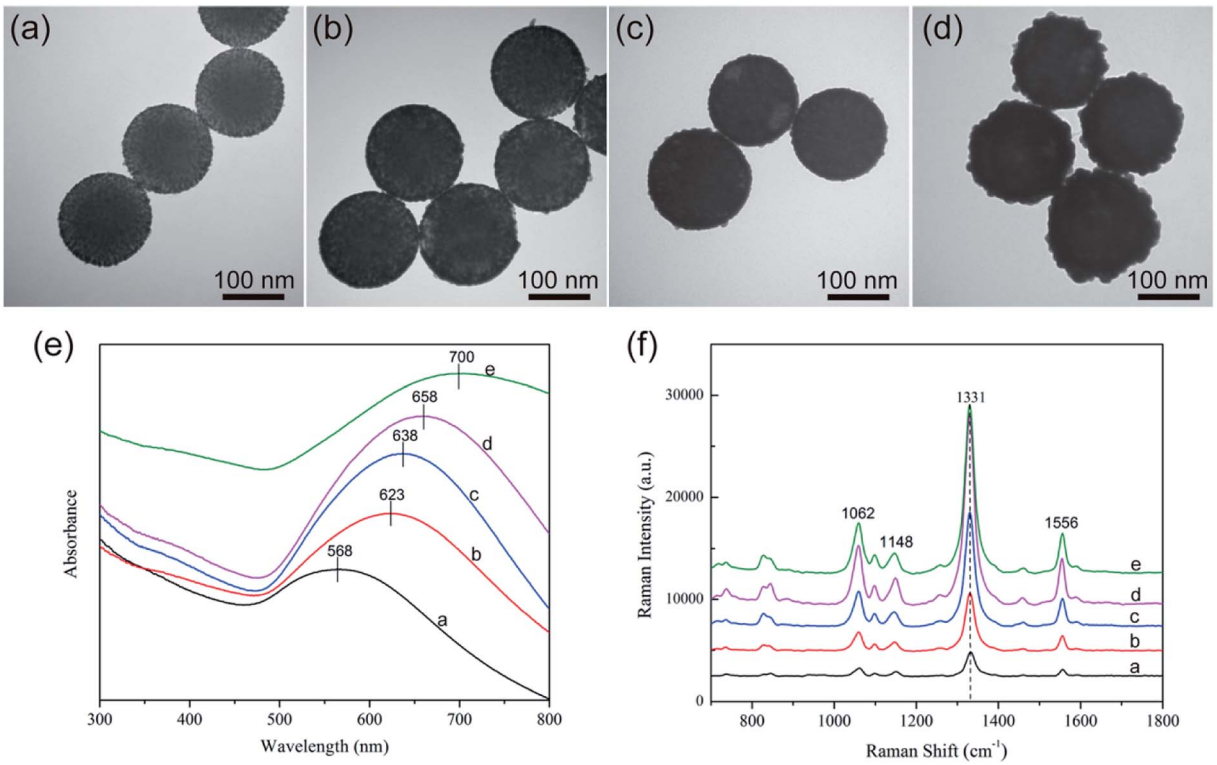

Fig. 3 TEM images of SiO_2@Au NPs synthesized with different $HAuCl_4$ concentrations: (a–d) 0.01, 0.02, 0.03, and 0.04 mM $HAuCl_4$. (e) UV-vis spectra of SiO_2@Au synthesized with different $HAuCl_4$ concentrations: curves (a–e) 0, 0.01, 0.02, 0.03, and 0.04 mM $HAuCl_4$ and the corresponding Raman spectra of DTNB (f).

potential to be active SERS substrate for greatly enhancing the SERS signal of molecules adsorbed on them.

Upon modification with Raman report molecules and detection antibodies, the monodisperse SiO_2@Au NPs must be efficient SERS tags for highly reproducible SERS immunoassays due to the integration of high SERS activity of the Au nanoshell and the homogeneity and stability of SiO_2 NPs (Fig. 6a). SERS-based LFA strip is a recently reported analytical technique to

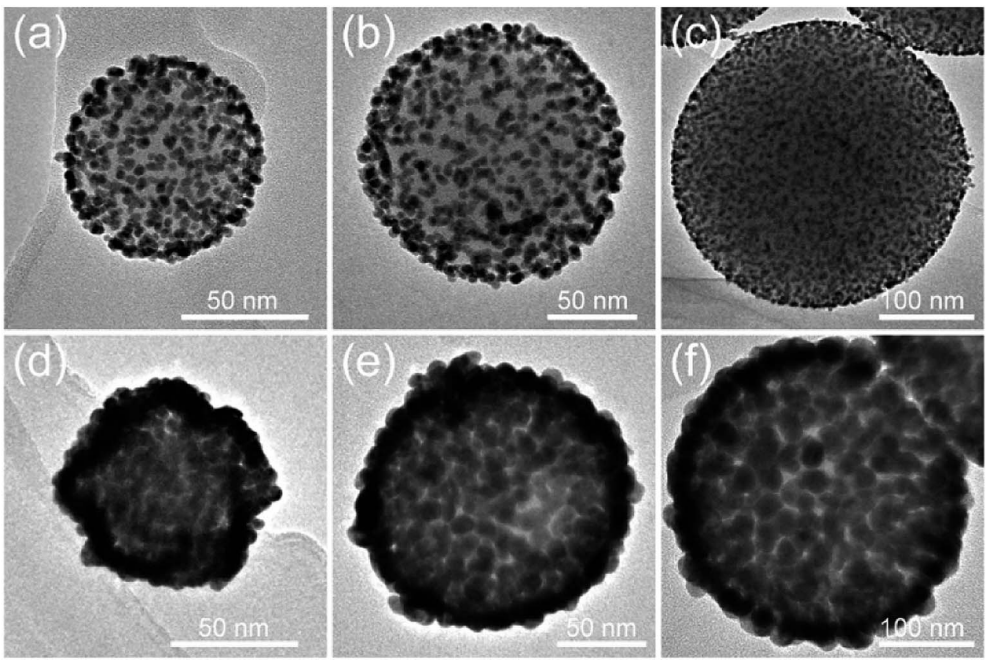

Fig. 4 (a–c) TEM images of single SiO_2–Au seed with different sizes: (a) 70, (b) 150, and (c) 300 nm and their corresponding fabricated SiO_2@Au NPs (d), (e), and (f), respectively.

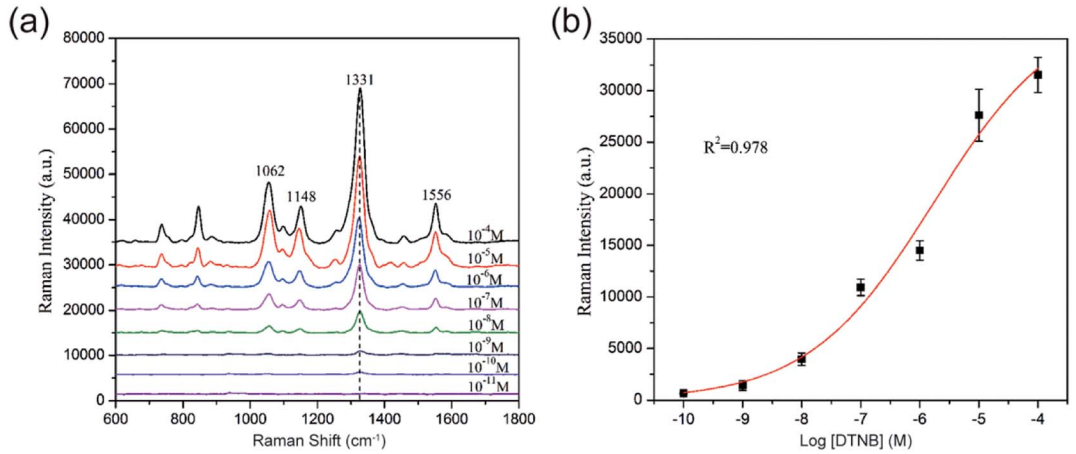

Fig. 5 (a) SERS spectra of DTNB measured with different concentrations on the SiO_2@Au NPs. (b) Calibration curve for DTNB at a concentration range of 10^{-4} M to 10^{-11} M obtained using SERS intensity at 1331 cm^{-1}. The error bars represent the standard deviations from five measurements.

overcome the shortcomings of conventional lateral flow assay, such as poor sensitivity and semiquantitative ability on the basis of colorimetric analysis.[25–27] The fundamental principle of SERS-based strip is the use of functional SERS tags instead of Au NPs. High-sensitivity and quantitative detection can be achieved by Raman spectroscopy because the intensity of the SERS signal is directly proportional to the number of SERS tags on the test line.

Fig. 6b represents the operating principle of the monodisperse SiO_2@Au NPs (80 nm) based SERS-LFA strip. Human IgM was selected as the model target antigen to explore the sensitivity of the proposed method. The representative SERS-LFA strip is composed of a sample loading pad, a conjugate pad, a NC membrane containing test line and control line, and an absorption pad. In our system, goat anti-human IgM antibody-labeled SiO_2@Au/DTNB NPs were dispensed onto the glass fiber paper as the conjugate pad, and the goat anti-human IgM antibody and donkey anti-goat immunoglobulin G (IgG) antibody were dispensed onto the NC membrane to form the test line and control line, respectively. When the sample solution containing the target human IgM passed through the conjugation pad, immunocomplexes (human IgM/SERS tags) were formed and continued migrating along the NC membrane until they reach the test line where they were captured by the previously immobilized anti-human IgM antibodies. Excess antibody-conjugated SiO_2@Au tags continued to migrate to the

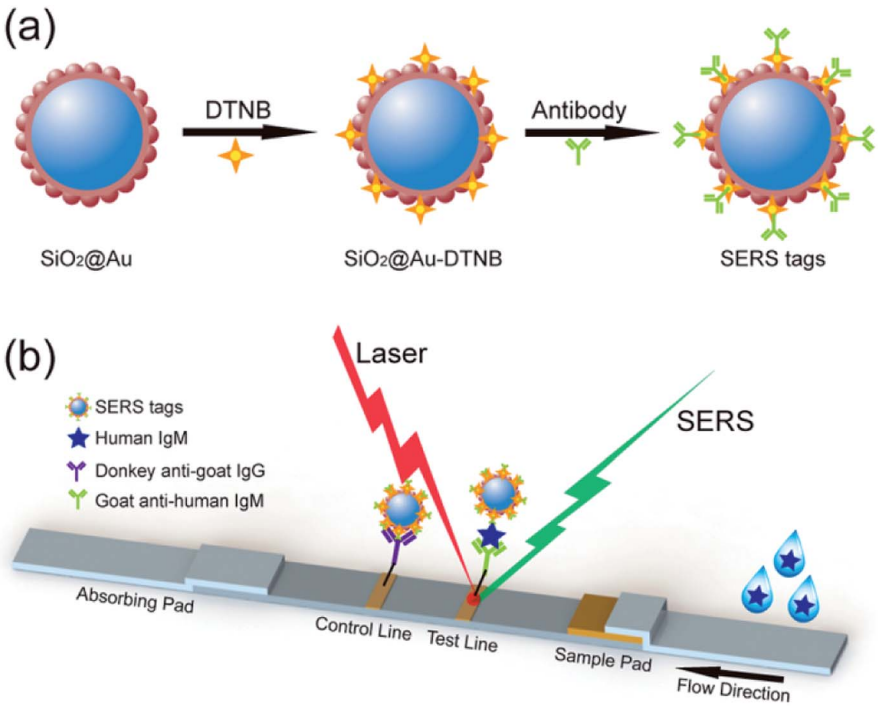

Fig. 6 (a) Synthesis route for SiO_2@Au SERS tags. (b) Schematic of SERS-based LFA strips for quantitative detection of human IgM.

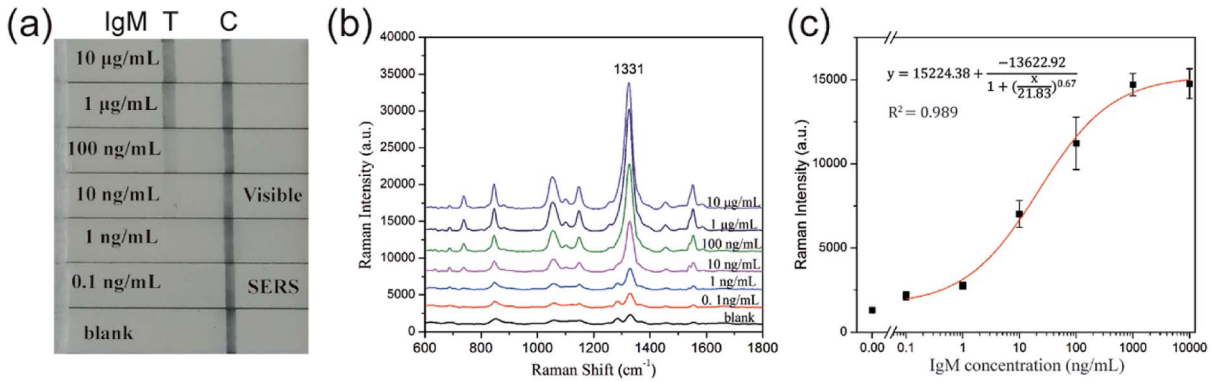

Fig. 7 (a) Photographs of SERS-based LFA strips in the presence of different concentrations of human IgM. (b) SERS spectra measured in the corresponding test lines. (c) Plot of the Raman intensity at 1331 cm^{-1} as a function of the logarithmic concentration of human IgM. The error bars represent the standard deviations from five measurements.

control line and were immobilized by the donkey anti-goat IgG antibody. Consequently, two dark bands appeared in the presence of the target human IgM (positive), whereas only the control line turned to a dark band in the absence of human IgM (negative). Quantitative detection of human IgM could be realized by detecting the SERS signal on the test line.

Human IgM was diluted within 10 000 ng mL^{-1} to 0.1 ng mL^{-1} as the sample solution, and PBST solution (10 mM PBS, 0.05% Tween-20) was used as blank control. As shown in Fig. 7a, the color of SERS tags captured by the test line was visualized and gradually decreased with decreasing human IgM concentration. The LOD of colorimetric method for detection of human IgM was found to be 10 ng mL^{-1}. Quantitative analysis was also conducted by measuring the characteristic Raman signals of the SERS tags on the test lines, and the Raman spectra are displayed in Fig. 7b. The Raman spectra were analyzed by plotting the intensity at 1331 cm^{-1} of DTNB as a function of the logarithm of the target human IgM concentration to generate a calibration curve (Fig. 7c). The LOD of the SERS-LFA strips based on the SiO_2@Au tags is 0.1 ng mL^{-1}, which was calculated as a 3 : 1 threshold ratio with respect to the blank control measurement. Using SiO_2@Au tags-based SERS LFA strip offers a 100-fold improvement in the detection limit compared with colorimetric analysis. Basing on these results, we demonstrated the high efficiency and great potential of monodisperse SiO_2@Au NPs as suitable SERS tags for SERS-based LFA strips. The specificity of the SERS-LFA strips was tested by a high concentration (1 μg mL^{-1}) of other proteins including human IgG and BSA. Fig. S5† shows the result of the specificity test. IgG and BSA did not show significant interference signals both in visualization and Raman spectrum analyses, whereas 100 ng mL^{-1} human IgM exhibited a strong signal. Hence, the SiO_2@Au tags-based SERS-LFA strip has good selectivity.

In summary, this work proposes a sonochemically assisted seed growth method for facile synthesis of monodisperse SiO_2@Au core–shell NPs with a complete Au shell. This method is a general route for preparing SiO_2@Au particles with sizes ranging from nanoscale to microscale levels. High-performance SiO_2@Au NPs were obtained from the intermediate product (SiO_2–Au seed) within 5 min through sonication. The obtained SiO_2@Au NPs were highly uniform in size and shape and exhibited satisfactory SERS activity. Hence, these NPs could be ideal SERS tags for various SERS based immunoassays. The small SiO_2@Au NPs (80 nm) with light weight and good dispersibility were also successfully applied to SERS-based LFA strip for human IgM rapid detection, with limit of detection as low as 0.1 ng mL^{-1}. We expect that high-performance SiO_2@Au NPs SERS tags can be used for actual detection.

Conflicts of interest

The authors report no conflicts of interest in this work.

Acknowledgements

This work was supported by Grants from the National Natural Science Foundation of China (No. 81230089 and 51605486), and Beijing Municipal Science & Technology Commission (No. Z161100000116040).

References

1 M. Kim, S. M. Ko and J. M. Nam, *Nanoscale*, 2016, **8**, 11707–11717.
2 S. Moraes Silva, R. Tavallaie, L. Sandiford, R. D. Tilley and J. J. Gooding, *Chem. Commun.*, 2016, **52**, 7528–7540.
3 V. P. Zharov, *Nat. Photonics*, 2011, **5**, 110–116.
4 X. Zhang, M. Wei, B. Lv, Y. Liu, X. Liu and W. Wei, *RSC Adv.*, 2016, **6**, 35001–35007.
5 C. Wang, J. Wang, M. Li, X. Qu, K. Zhang, Z. Rong, R. Xiao and S. Wang, *Analyst*, 2016, **141**, 6226–6238.
6 M. Bikram, A. M. Gobin, R. E. Whitmire and J. L. West, *J. Controlled Release*, 2007, **123**, 219–227.
7 Y. An, G. Zhu, W. Bi, L. Lu, C. Feng, Z. Xu and W. Zhang, *Anal. Chim. Acta*, 2017, **966**, 54–61.
8 K. Zhang, L. L. Xu, J. G. Jiang, N. Calin, K. F. Lam, S. J. Zhang, H. H. Wu, G. D. Wu, B. Albela, L. Bonneviot and P. Wu, *J. Am. Chem. Soc.*, 2013, **135**, 2427–2430.
9 A. M. Asadirad and N. R. Branda, *J. Am. Chem. Soc.*, 2015, **137**, 2824–2827.

10 L. Lu, I. Randjelovic, R. Capek, N. Gaponik, J. Yang, H. Zhang and A. Eychmüller, *Chem. Mater.*, 2005, **17**, 5731–5736.
11 T. Pham, J. B. Jackson, N. J. Halas and T. R. Lee, *Langmuir*, 2002, **18**, 4915–4920.
12 C.-L. Li, J.-K. Chen, S.-K. Fan, F.-H. Ko and F.-C. Chang, *ACS Appl. Mater. Interfaces*, 2012, **4**, 5650–5661.
13 Y. Lu, G. Yao, K. Sun and Q. Huang, *Phys. Chem. Chem. Phys.*, 2015, **17**, 21149–21157.
14 P. Dobrowolska, A. Krajewska, M. Gajda-Rączka, B. Bartosewicz, P. Nyga and B. Jankiewicz, *Materials*, 2015, **8**, 2849–2862.
15 Y. Lu, J. Zhong, G. Yao and Q. Huang, *Sens. Actuators, B*, 2018, **258**, 365–372.
16 R. Wang, X. Ji, Z. Huang, Y. Xue, D. Wang and W. Yang, *J. Phys. Chem. C*, 2016, **120**, 377–385.
17 L. Gomez, M. Arruebo, V. Sebastian, L. Gutierrez and J. Santamaria, *J. Mater. Chem.*, 2012, **22**, 21420–21425.
18 F. Ke, L. Wang and J. Zhu, *Nanoscale*, 2015, **7**, 1201–1208.
19 C. Song, L. Min, N. Zhou, Y. Yang, B. Yang, L. Zhang, S. Su and L. Wang, *RSC Adv.*, 2014, **4**, 41666–41669.
20 C. Wang, M. Li, Q. Li, K. Zhang, C. Wang, R. Xiao and S. Wang, *RSC Adv.*, 2017, **7**, 13138–13148.
21 J. Tharion, J. Satija and S. Mukherji, *RSC Adv.*, 2014, **4**, 3984–3991.
22 C. C. Lin and C. W. Chang, *Biosens. Bioelectron.*, 2014, **51**, 297–303.
23 C. Wang, J. Xu, J. Wang, Z. Rong, P. Li, R. Xiao and S. Wang, *J. Mater. Chem. C*, 2015, **3**, 8684–8693.
24 Z. Wang, S. Zong, W. Li, C. Wang, S. Xu, H. Chen and Y. Cui, *J. Am. Chem. Soc.*, 2012, **134**, 2993–3000.
25 X. Wang, N. Choi, Z. Cheng, J. Ko, L. Chen and J. Choo, *Anal. Chem.*, 2017, **89**, 1163–1169.
26 L. Blanco-Covian, V. Montes-Garcia, A. Girard, M. T. Fernandez-Abedul, J. Perez-Juste, I. Pastoriza-Santos, K. Faulds, D. Graham and M. C. Blanco-Lopez, *Nanoscale*, 2017, **9**, 2051–2058.
27 J. Hwang, S. Lee and J. Choo, *Nanoscale*, 2016, **8**, 11418–11425.